ACS Catalysis

Research Article

pubs.acs.org/acscatalysis

Superior Stability of Au/SiO_2 Compared to Au/TiO_2 Catalysts for the Selective Hydrogenation of Butadiene

Nazila Masoud,[†] Laurent Delannoy,[‡] Herrick Schaink,[†] Ad van der Eerden,[†] Jan Willem de Rijk,[†] Tiago A. G. Silva,[‡] Dipanjan Banerjee,[§,∥] Johannes D. Meeldijk,[⊥] Krijn P. de Jong,[†] Catherine Louis,[‡] and Petra E. de Jongh*[,†]

[†]Inorganic Chemistry and Catalysis, Debye Institute for Nanomaterials Science, Utrecht University, 3584 CG Utrecht, The Netherlands

[‡]Laboratoire de Réactivité de Surface, Sorbonne Universités, UPMC Univ Paris 06, UMR CNRS 7197, 4 Place Jussieu, Case 178, F-75252 Paris, France

[§]Dutch−Belgian Beamline (DUBBLE), ESRF-The European Synchrotron, CS40220, 38043 CEDEX 9 Grenoble, France

[∥]Department of Chemistry, KU Leuven, Celestijnenlaan 200F, Box 2404, 3001 Leuven, Belgium

[⊥]Electron Microscopy Facility, Debye Institute for Nanomaterials Science, Utrecht University, 3584 CG Utrecht, The Netherlands

Supporting Information

ABSTRACT: Supported gold nanoparticles are highly selective catalysts for a range of both liquid-phase and gas-phase hydrogenation reactions. However, little is known about their stability during gas-phase catalysis and the influence of the support thereon. We report on the activity, selectivity, and stability of 2−4 nm Au nanoparticulate catalysts, supported on either TiO_2 or SiO_2, for the hydrogenation of 0.3% butadiene in the presence of 30% propene. Direct comparison of the stability of the Au catalysts was possible as they were prepared via the same method but on different supports. At full conversion of butadiene, only 0.1% of the propene was converted for both supported catalysts, demonstrating their high selectivity. The TiO_2-supported catalysts showed a steady loss of activity, which was recovered by heating in air. We demonstrated that the deactivation was not caused by significant metal particle growth or strong metal−support interaction, but rather, it is related to the deposition of carbonaceous species under reaction conditions. In contrast, all the SiO_2-supported catalysts were highly stable, with very limited formation of carbonaceous deposits. It shows that SiO_2-supported catalysts, despite their 2−3 times lower initial activities, clearly outperform TiO_2-supported catalysts within a day of run time.

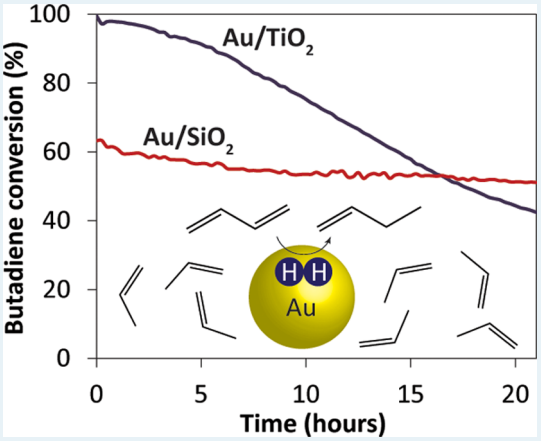

KEYWORDS: *gold, supported nanoparticles, selective hydrogenation, butadiene, catalyst, stability*

1. INTRODUCTION

Gold catalysts are very attractive due to their unique properties such as a high activity at low temperatures for CO oxidation and a high selectivity for a wide range of oxidation and hydrogenation reactions.[1−11] Gold is an active catalyst for selective hydrogenation of, for instance, α,β-unsaturated aldehydes,[12] nitroaromatics,[13] and acetylene in the presence of an excess of ethylene[14] as well as butadiene in the presence of an excess of alkenes.[15] Strikingly, for the selective hydrogenation of butadiene, Au is highly selective for hydrogenation of butadiene without overhydrogenation to alkanes.[16] The activity of Au catalysts for hydrogenation reactions has been investigated extensively and is affected by many factors[17−20] such as particle size, nature of the support, and catalyst preparation method. For example, Fujitani et al.[21] reported that smaller Au nanoparticles supported on TiO_2 are more active for the H_2−D_2 exchange reaction than larger particles in the range of 3.4−10 nm particles. H_2 dissociation is believed to be the rate determination step for the hydrogenation reaction catalyzed by Au.[22−24] Corma et al.[25] postulated, on the basis of computational studies, that H_2 dissociation is also influenced by the nature of the support, and Louis et al.[26] reported that Au/Al_2O_3 catalysts prepared by anionic adsorption were less active than similar catalysts prepared by deposition−precipitation with urea for the selective hydrogenation of butadiene.

Studies often do not mention the stability of the investigated catalysts, though the potential application of Au catalysts

Received: May 2, 2017
Revised: July 14, 2017
Published: July 14, 2017

DOI: 10.1021/acscatal.7b01424
ACS Catal. 2017, 7, 5594−5603

strongly depends on their stability.[27] The stability of Au catalysts has been studied for CO oxidation,[28−30] water gas shift reaction,[31] benzyl alcohol oxidation,[32] epoxidation,[33] PROX reaction,[34] acetylene hydrogenation,[35−39] acetylene hydrochlorination,[40] and *p*-chloronitrobenzene hydrogenation.[41] These studies always compared catalysts on the same type of support, usually CeO_2, Al_2O_3, or TiO_2, with Au/TiO_2 catalysts discussed in the most detail. Au/TiO_2 catalysts are known to deteriorate during storage as they are light and moisture sensitive.[42] They deactivate fast under oxidizing conditions,[29] for example, during CO oxidation, with particle growth and passivation of active sites by carbonates as major deactivation pathways.[43] Under reducing conditions, deactivation due to carbonaceous deposit formation is most dominant. For example, Choudhary et al.[35] report that Au/TiO_2 catalysts for acetylene hydrogenation lost activity with time due to the carbon deposition. Louis et al.[26] suggested that Au catalyst deactivation might depend on the nature of the support for hydrogenation of butadiene: Au on TiO_2 showed the highest deactivation rate in a series of Au on TiO_2, Al_2O_3, ZrO_2, and CeO_2. Sárkány[37] also reported faster deactivation of Au/TiO_2 than for Au supported on SiO_2 for the acetylene hydrogenation. Furthermore, it is known for metal nanoparticles on reducible supports like TiO_2 and ZnO, that strong interaction between metal nanoparticles and the support can be an important activity loss mechanism when heated to high temperatures under reducing conditions.[29,44−48]

SiO_2 is a nonreducible oxidic support, which is widely used in heterogeneous catalysis.[49,50] It is available with different specific surface areas and porosities and can also be prepared as ordered mesoporous structures like SBA15[51] with uniform hexagonally arranged pores and a narrow pore size distribution. In contrast to Au/TiO_2 catalysts, Au/SiO_2 catalysts have been minimally studied mainly due to difficulties in catalyst preparation. There are a few methods for the deposition of Au on SiO_2 that lead to small Au particles,[52,53] as by applying typical deposition methods large particles are formed, due to the low point of zero charge of this support.[54] Alternative deposition methods of Au on SiO_2 are more complicated, such as physical preparation methods which can change the surface properties[55] and colloidal methods which are often associated with interfering organic ligands[56] or Cl residues.[53]

As mentioned before, the effectiveness of Au catalysts for hydrogenation reactions is affected by the catalyst preparation method. Different preparation methods lead to different structural properties of the catalysts. Especially, particle size, shape, and contaminant concentration like chloride[26,57−59] are parameters that are likely to affect the Au catalyst performance. Hence, a comparison of the activity and stability of metal catalysts on different supports requires precision in catalyst preparation,[60] preferably using the same method to deposit the same metal nanoparticles on different supports.[61−64] We used a method that is well established for the preparation of Au/SiO_2 catalysts[53] to also prepare similar Au nanoparticles on TiO_2 supports. As a test reaction, we chose the selective hydrogenation of butadiene in propene feedstocks for polyolefin production. Since impurities like butadiene poison the polymerization catalysts, these dienes must be hydrogenated to concentrations less than 100 ppm, without significant hydrogenation of alkenes in the reaction mixture.[15]

In this study, we present the selectivity, activity, and stability of the Au/TiO_2 catalysts for the selective hydrogenation of butadiene and compare it to Au catalysts supported on SiO_2. To the best of our knowledge, this is the first study to compare the stability during continuous time-on-stream for Au catalysts prepared by the same method but on different supports for a hydrogenation reaction. We provide insight into the deactivation mechanisms for supported Au catalysts in gas-phase hydrogenation reactions. Interestingly, Au/SiO_2 catalysts clearly outperform Au/TiO_2 catalysts after a certain time-on-stream.

2. EXPERIMENTAL SECTION

2.1. Catalyst Preparation. Commercially available TiO_2 (P25, Degussa, BET surface area of 50 $m^2 \cdot g^{-1}$) was chosen, which contains anatase and rutile phases in a ratio of about 3:1. For SiO_2 supports, commercially available Aerosil 50 (Evonik, BET surface area of 50 $m^2.g^{-1}$, denoted as SiO_2-A50) and Aerosil 300 (Evonik, BET surface area of 300 $m^2 \cdot g^{-1}$, denoted as SiO_2-A300) were used. Additionally, SBA15 was prepared by the method of Sayari et al.[51] In a typical preparation, poly(ethylene oxide)-*block*-poly(propylene oxide)-*block*-poly(ethylene oxide) triblock copolymer (4.0 g, $EO_{20}PO_{70}EO_{20}$, Pluronic P123, M_{av} of 5800 D, Sigma-Aldrich) was dissolved in mixture of diluted HCl (120 g, 2 M) and water (30 g) at room temperature. After at least 45 min at 35 °C, tetraethoxysilane (8.5 g) was added and stirred for 5 min. After 20 h at 38 °C under static conditions, the cloudy mixture was kept at 90 °C for 24 h. The precipitate was filtered and washed at room temperature (RT) until all chloride ions are removed and was dried at 60 °C in static air overnight. Then, the precipitate was calcined at 550 °C in static air for 6 h to yield SBA15.

All supports (3 g) were functionalized using aminopropyl triethoxysilane (APTES). First, they were dried at 140 °C under vacuum for 24 h. Then, dry toluene (50 mL) and APTES (0.27 g for TiO_2, 0.18 g for SiO_2-A50, 1 g for SiO_2-A300, and 3 g for SBA15) were added. We added the amount of APTES needed for covering the support surface based on the BET surface area of the supports, considering five OH groups per nm^2 for TiO_2 and three OH groups per nm^2 for SiO_2.[65] The mixture was refluxed for 24 h at 110 °C in a N_2 atmosphere. The functionalized supports were recovered by centrifugation, washed with ethanol (40 mL) at RT twice, and dried at 60 °C in static air overnight.

All catalysts were prepared by the method of Mou et al. for the deposition of Au on SiO_2.[53] The functionalized supports (1 g) were dispersed in water (15 mL, doubled distilled). To deposit 1 wt % Au on TiO_2 and SiO_2-A50, 2 wt % Au on SiO_2-A300, and 4 wt % Au on SBA15, an appropriate amount of an aqueous Au solution (0.06 M $HAuCl_4 \cdot 3H_2O$, Sigma-Aldrich) was added. The mixture was stirred at room temperature for 2 h, and the powder was recovered by centrifugation and washed with H_2O (40 mL) at RT twice. Then, the powder was redispersed in water (15 mL) and reduced by a rapid addition of an excess of a reducing agent (10 mL, 0.2 M $NaBH_4$) under vigorous stirring at RT. After 20 min, the product was collected by centrifugation, washed with water (40 mL) at RT five times, and dried at 60 °C in static air overnight. To eliminate the organic groups, the catalysts were calcined at 500 °C in static air for 4 h. The catalysts are denoted as Au/TiO_2, Au/SiO_2-A50, Au/SiO_2-A300, and Au/SBA15.

2.2. Characterization. Nitrogen physisorption measurements were done at −196 °C (77 K) (Micromeritics, TriStar 3000). Thermogravimetric analysis (TGA) was performed on a PerkinElmer (Pris 1) connected to a mass detector on around 10 mg of the powder sample heated for 30 min at 150 °C and

DOI: 10.1021/acscatal.7b01424
ACS Catal. 2017, 7, 5594−5603

Table 1. Structural Properties of the Au Catalysts

	BET surface area ($m^2 \cdot g^{-1}$)	Au loading (wt %)	Cl content (wt %)	TEM particle size (nm) number-averaged[a]	TEM particle size (nm) surface-averaged[b]	XRD crystallite size (nm)
Au/TiO_2	50	0.5	0.19	3.8 ± 0.9	4.3	-
Au/SiO_2-A50	50	0.6	0.17	3.1 ± 1.6	5.8	-
Au/SiO_2-A300	300	1.7	0.65	2.9 ± 1.1	3.8	4.1
Au/SBA15	800	3.6	0.11	2.6 ± 0.7	3.0	3.2

[a]Calculated as $\sum n_i d_i / \sum n_i$, [b]Calculated as $\sum n_i d_i^3 / \sum n_i d_i^2$, d_i is the particle diameter

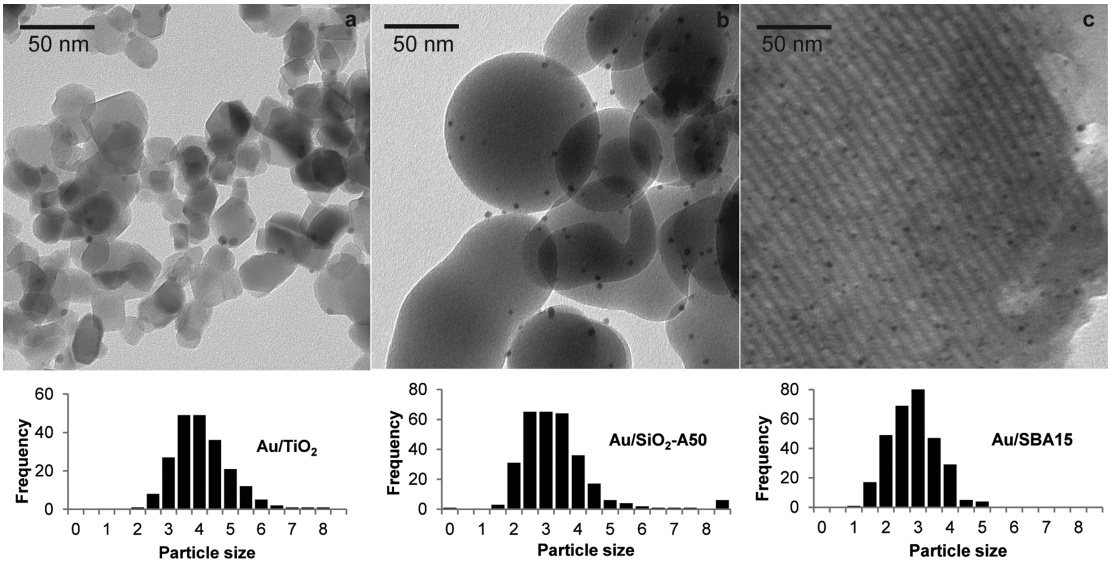

Figure 1. Transmission electron micrographs and particle size histograms of (a) 0.5 wt % Au/TiO_2, (b) 0.6 wt % Au/SiO_2-A50, and (c) 3.6 wt % Au/SBA15.

further heated to 800 °C (5 °C·min^{-1}) under a flow of oxygen (10 mL·min^{-1}) over the sample. Elemental analysis was performed on an inductively coupled plasma-mass spectrometry analysis (Mikroanalytisches Laboratorium Kolbe, Germany). Transmission electron microscopy (TEM) imaging was performed on a Tecnai 12 (FEI) microscope operated at 120 kV. Particle sizes were determined from the TEM micrographs by measuring the sizes of typically 200−300 individual particles on different areas of the sample. High-angle annular dark-field scanning transmission electron microscopy (HAADF-STEM) was performed on a Talos F200X microscope operated at 200 kV. Energy-dispersive X-ray (EDX) spectroscopy was performed by four windowless SuperX EDX-detectors with a resolution of 128 eV arranged around the sample. STEM image processing and identification of the EDX signal was carried out using Tecnai Imaging Analysis (TIA) software.

X-ray diffraction (XRD) analysis was carried out with a Bruker D2 phaser with Co Kα source. The extended X-ray absorption fine structure spectroscopy (EXAFS) spectra were acquired at the Dutch-Belgian beamline (DUBBLE) of the synchrotron facility in Grenoble and at the ROCK beamline of the Soleil synchrotron radiation facility, both in France. The measurements at DUBBLE were performed in fluorescence mode using a Si (111) monochromator at RT on a pellet sample under atmospheric condition.[66] X-ray flux was 3×10^{10} photons.s^{-1}. The measurement at ROCK was performed in transmission mode using Si(111) at 8.0 keV with flux of 2×10^{12} photons.s^{-1} at RT on a powder sample under atmospheric condition. The collected EXAFS spectra were background corrected and analyzed using XDAP software. The Au coordination number (Au CN), the Au−Au distance (R), the difference of the Debye−Waller factor from the reference ($\Delta\sigma^2$), and the correction of the threshold energy (ΔE^0) were treated as free parameters during the fitting. The quality of the fit was estimated from the values of k^3 variance (V_{k3}) which represents the difference between the experimental data and fitted spectra in the fitted range. Low values of variance indicate a good agreement between experimental data and the fit.

2.3. Catalysis. The hydrogenation of butadiene was performed in a Pyrex plug flow reactor (internal diameter of 4 mm). Prior to reaction, the catalysts (sieve fraction of 150−212 μm) were reduced in situ under pure H_2 (50 mL·min^{-1}) from RT to 450 °C (ramp 3 °C·min^{-1}) and kept at 450 °C for 180 min, and then cooled to RT. Ex situ reduction of the catalysts was performed under the same conditions to analyze the properties of the catalysts before the catalytic test. The reaction mixture consisted of 0.3% butadiene, 30% propene, 20% hydrogen, and helium for balance with a flow rate of 50 mL·min^{-1} (normal temperature and pressure conditions). The product mixtures were analyzed every 15 min with online gas chromatography.

After in situ reduction, to test the activity and the selectivity, the catalyst (100 mg) was exposed to the reaction mixture (gas hourly space velocity (GHSV) is 20 000 h^{-1} for Au/TiO_2 and 11700 h^{-1} for Au/SiO_2), while the catalyst was heated at a rate of 1 °C·min^{-1}, from RT up to 300 °C. Turnover frequencies (TOF) were calculated from the activity × M_{Au}/D, where M_{Au} is the Au molecular weight, and the dispersion (D) is calculated

DOI: 10.1021/acscatal.7b01424
ACS Catal. 2017, 7, 5594−5603

by $6(\nu_m/a_m)/d_{VA}$. Here, a_m is the area occupied by a surface atom, ν_m is the volume occupied by an atom in bulk metal, and d_{VA} is the surface-averaged particle size.[67]

To test the stability, either the Au/TiO_2 or Au/SiO_2-A50 (150 mg), or the Au/SiO_2-A300 (100 mg), or the Au/SBA15 (50 mg) were loaded to the reactor. For SiO_2-supported catalysts that have different Au loadings, different weights of catalyst were used to have high initial conversions but below full conversion. The maximum amount of SiO_2-supported catalysts that can be loaded in the reactor is 150 mg. After in situ reduction, the reactor was cooled down to 200 °C, and the catalytic reaction was performed for 16 h at this temperature. To perform the stability tests on the Au/TiO_2 and Au/SiO_2-A50 with the same GHSV, the catalytic beds were adjusted to the same height: the Au/TiO_2 (60 mg) was diluted with bare TiO_2 (280 mg) and the Au/SiO_2-A50 (60 mg) was diluted with bare SiO_2 (105 mg). Reactivation tests were performed after a stability test on the Au/TiO_2 catalyst (60 mg) in situ by passing a flow of dry air or H_2 (50 mL·min^{-1}) for 1.5−3 h through the spent catalyst at 450 °C. In all experiments, carbon was balanced within the accuracy of the GC analysis, which is 1%. All catalytic tests and analytical measurements were performed at least twice to ensure reproducibility of the results, in general the deviations for instance in absolute conversion levels at a given temperature were less than 10%.

3. RESULTS AND DISCUSSION

3.1. Structural Characterization. Table 1 presents the structural properties for the relevant Au on TiO_2 and on SiO_2 catalysts. For the first two catalysts, Au/TiO_2 and Au/SiO_2-A50, we aimed for similar structural properties. The BET surface areas of the TiO_2 and SiO_2-A50 supports were similar (50 $m^2.g^{-1}$). Elemental analysis showed similar Au loadings and Cl contents for these two catalysts. Transmission electron microscopy (TEM) (Figure 1a,b) showed a similar particle size for Au nanoparticles on TiO_2 and SiO_2 supports. The size distribution of Au/SiO_2-A50 is slightly broader, as occasionally much larger particles are observed in the sample. This leads to a somewhat larger surface-averaged particle size for this catalyst. The error in surface-averaged particle sizes is between 0.1 and 0.4 nm (Figure S1). However, for the Au/SiO_2-A50 the error was larger, due to a few larger particles in some areas of the sample. Crystallite sizes could not be derived from XRD for the Au/TiO_2 and Au/SiO_2-A50 catalysts due to their low metal loadings.

The accuracy of the particle size for the Au/TiO_2 obtained by TEM is limited by the fact that Au and TiO_2 display little contrast in bright-field TEM. Hence, we employed high-angle annular dark-field scanning transmission electron microscopy (HAADF-STEM, Figure 2). Clusters of smaller than 1 nm were visible additionally in Au/TiO_2 (red arrows in Figure 2a), while no small clusters were detected in Au/SiO_2-A50. Energy-dispersive X-ray spectroscopy analysis confirmed that small clusters consist of Au (Figure S2). To validate the particle sizes for Au/TiO_2 and Au/SiO_2-A50, extended X-ray absorption fine structure spectroscopy (EXAFS) measurements were performed on the as-prepared samples. Detailed calculations can be found in the Supporting Information (S.1). EXAFS gives an average Au coordination number of 9.2 for the Au/TiO_2 and 10.9 for the Au/SiO_2-A50, which corresponds to particle size of 1.9 and 4.0 nm, respectively. The fact that the EXAFS particle size (1.9) is smaller than the one obtained by TEM (4.3 nm) confirms that next to the larger nanoparticles, small Au clusters

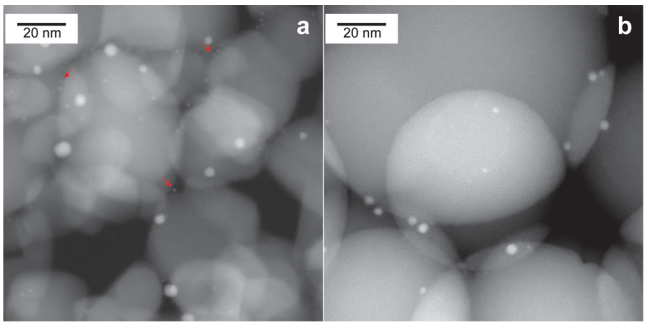

Figure 2. High-angle annular dark-field scanning transmission electron micrographs of (a) 0.5 wt % Au/TiO_2 and (b) 0.6 wt % Au/SiO_2-A50, red arrows show Au clusters of smaller than 1 nm.

are present on Au/TiO_2, which can be explained by a strong interaction of the Au negative precursor with the TiO_2 surface. In summary, the Au/TiO_2 and Au/SiO_2-A50 catalysts present similar Au loading, support surface area, and particle size, except the fact that Au/TiO_2 also contains a minority of small Au clusters.

For the Au/SiO_2 catalysts, different support surface areas and pore structures were used. Thermogravimetric analysis (TGA) (Figure S3) showed that the number of functional groups on the supports scales linearly with the support specific surface areas. For example, it is two times higher for SBA15 than for SiO_2-300. The number of functional groups on the support limits the maximum metal loading that can be achieved. Hence, we targeted a higher Au loading for the Au/SBA15 catalyst (800 m^2/g) than for the Au/SiO_2-A300 and Au/SiO_2-A50 catalysts (300 m^2/g and 50 m^2/g, respectively). In all cases the achieved loading was close to the targeted loading. SBA15 has a pore size of 8 nm and an ordered mesoporous structure (Figure S4). TEM shows Au nanoparticles inside the pores of the SBA15 (Figure 1c). Crystallite sizes obtained by XRD (Table 1 and Figure S5) confirmed particle sizes obtained by TEM for the Au/SiO_2-A300 and Au/SBA15 catalysts. Note that the EXAFS particle size for Au/SiO_2-A50 (4.0 nm) is also in the range of sizes for Au nanoparticles on other silica supports (3−4 nm). Thus, the Au/SiO_2-A50, Au/SiO_2-A300, and Au/SBA15 catalysts have the same chemical nature of the support, but different support specific surface areas and pore structures, which influences the Au loading but has almost no influence on the Au particle size.

3.2. Catalytic Selectivity and Activity. The selectivity and activity of the catalysts were assessed by measuring the concentrations of the reactants and products during reaction while the temperature is increasing gradually. Figure 3 shows the evolution of the concentrations of all reactants and products for the Au/TiO_2 and Au/SiO_2-A50 catalysts in the temperature range of 50−300 °C. The main products of hydrogenation of butadiene for both catalysts, in order, are 1-butene, cis-2-butene, and trans-2-butene. This is consistent with the earlier reported selectivities for Au catalysts for the hydrogenation of butadiene.[26,68]

For the Au/TiO_2 catalyst (Figure 3a), at 240 °C the remaining butadiene concentration in the product stream is less than 100 ppm, while the propane concentration is only 180 ppm, and the butane concentration is below the detection limit. This means that while more than 96.7% of the butadiene is hydrogenated, only 0.1% of the propene is hydrogenated, despite a 2 orders of magnitude higher concentration. In other

DOI: 10.1021/acscatal.7b01424
ACS Catal. 2017, 7, 5594−5603

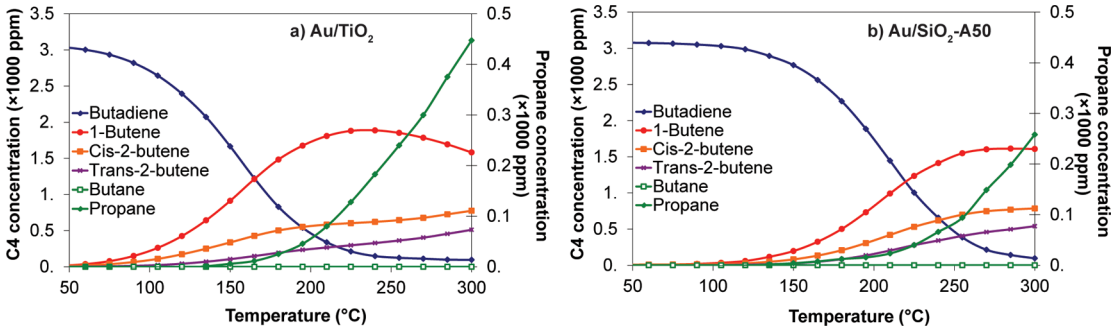

Figure 3. Concentrations of reactants and products for (a) 0.5 wt % Au/TiO_2 (b) 0.6 wt % Au/SiO_2-A50 (both 100 mg) for the hydrogenation of butadiene while heating from 50 to 300 °C with 1 °C·min^{-1}. The reaction mixture consisted of 0.3% butadiene, 30% propene, 20% hydrogen, and He for balance, and flow rate was 50 mL·min^{-1}.

words the selectivity for hydrogenation is above 99.9% toward the butadiene; the Au/TiO_2 catalyst is very selective. This selectivity is similar to that reported for Au/TiO_2 and Au/Al_2O_3 prepared via deposition-precipitation with urea (DPU).[26]

For the Au/SiO_2-A50 catalyst (Figure 3b), at 285 °C, the remaining butadiene concentration is less than 100 ppm (96.7% of the butadiene is hydrogenated), while the propane concentration is 200 ppm (only 0.1% of the propene is hydrogenated), and the butane concentration is not detectable. In comparison to the Au/TiO_2 catalyst, the Au/SiO_2-A50 catalyst reaches the same conversion of butadiene (96.7%) at a higher temperature (285 °C instead of 240 °C) and is therefore less active. However, at the same conversion of butadiene, for the Au/TiO_2 and Au/SiO_2-A50 catalysts, propane concentrations are similar (200 and 180 ppm, respectively), which means the Au/SiO_2-A50 catalyst is as selective as the Au/TiO_2 catalyst toward hydrogenation of butadiene.

Table 2 presents an overview of the activities and turnover frequencies (TOF) of the catalysts at 120 °C obtained from

Table 2. Particle Sizes, Activity, and TOF for Au/TiO_2 and Au/SiO_2 Catalysts

	particle size (nm)	activity (μmol·s^{-1}·g$_{Au}^{-1}$) at 120 °C	TOF (10^{-3} s^{-1}) at 120 °C
Au/TiO_2	1.9[a]	48	15
Au/SiO_2-A50	4.0[a]	6	4
Au/SiO_2-A300	3.8[b]	6	4
Au/SBA15	3.0[b]	9	5

[a]EXAFS particle size. [b]TEM particle size.

measuring the butadiene conversion during a temperature ramp (Figure 3 and Figure S6). Studied on the kinetics of hydrogenation of butadiene in the presence of an excess of propene at different temperatures[16] shows that at 120 °C the conversion of butadiene is kinetically controlled, the reaction rate is close to zero order in butadiene concentration and decreases slightly with increasing propene concentration due to competitive adsorption. The estimation of the average TOF based on the EXAFS particle size for the Au/TiO_2 catalyst is 15 × 10^{-3} s^{-1}. This TOF is comparable to the literature values for Au/TiO_2 catalysts: A TOF of 20 × 10^{-3} s^{-1} at 120 °C is reported for Au/TiO_2 prepared via DPU.[26]

The TOF is 4 × 10^{-3} s^{-1} for the Au/SiO_2-A50 catalyst at 120 °C (Table 2), which is lower than that of the Au/TiO_2 catalyst (15 × 10^{-3} s^{-1}). A lower activity for Au/SiO_2 than for Au/TiO_2 for the hydrogenation of butadiene has been also reported by Haruta et al. (TOF of 6 × 10^{-3} s^{-1} for the Au/SiO_2 versus 20 × 10^{-3} s^{-1} for the Au/TiO_2 (particle sizes of 7.0 ± 3.0 and 3.5 ± 1.3, respectively) at 150 °C).[69,70] The lower activity seems specific for SiO_2 supports since higher and very similar activities were found for Au on Al_2O_3, ZrO_2 and CeO_2 as well as for Au on TiO_2 by Louis et al.[26] Kinetic studies showed that the apparent activation energy for Au catalysts on different supports, including SiO_2 and TiO_2, does not depend on the support,[26,71] suggesting that similar active sites are present in all supported Au catalysts. There is consensus in literature that H_2 dissociation is the rate-determining step for hydrogenation reaction, but no clear consensus on which sites are the most active ones. Experimentally[21] and theoretically,[72,73] Au sites at the interface with the support are shown to be the most active ones. However, other experimental data[26] show no difference in activity for Au catalysts on a range of different supports (not including silica), suggesting that the most active sites are not Au sites at the support interface, but rather low-coordinated sites on the Au particles.[23−25,74] In any case, the higher average TOF on the nonsilica supports might be explained by the presence of additional highly active sites, either at the interface with the support, or low coordination surface sites. In the present study, particularly the small clusters that are exclusively present on the TiO_2 support might be an important factor in causing a higher activity for Au/TiO_2 than for Au/SiO_2.

To compare the activity and selectivity of the different Au/SiO_2 catalysts, the concentrations of butadiene and propane are given in Figure 4 (the concentrations of all reactants and products for the Au/SiO_2-A300 and Au/SBA15 catalysts in the temperature range of 50−300 °C are shown in Figure S6). The Au/SBA15, Au/SiO_2-A300, and Au/SiO_2-A50 catalysts reach the same conversion level of butadiene (>96.7%) at different temperatures: 195, 240, and 285 °C, respectively. Since the same mass of catalyst is used for each test (100 mg), this is due to the higher Au loading of the Au/SBA15 catalyst (3.6 wt %) in comparison to the Au/SiO_2-A300 (1.7 wt %) and Au/SiO_2-A50 (0.6 wt %) catalysts. The turnover frequencies are in the range of 4 to 5 × 10^{-3} s^{-1} for all the Au/SiO_2 catalysts at 120 °C. Hence, the Au/SiO_2 catalysts have similar intrinsic activities. At the same butadiene conversion (>96.7%), only 0.1% of the propene is converted to propane for the three Au/SiO_2 catalysts. Thus, all the Au/SiO_2 catalysts show similar selectivities for the hydrogenation of butadiene. Hence, the selectivity and the activity of the Au/SiO_2 catalysts are independent of the support surface area and pore structure.

DOI: 10.1021/acscatal.7b01424
ACS Catal. 2017, 7, 5594−5603

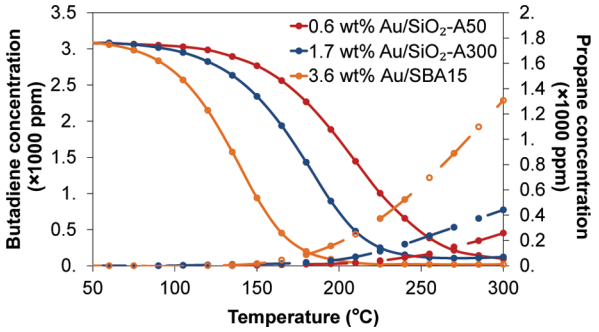

Figure 4. Concentrations of butadiene (solid lines) and propane (dashed lines) for Au/SiO_2 catalysts (all 100 mg) with loadings from 0.6 to 3.6 wt % and on SiO_2 with different surface areas and pore structures while heating from 50 to 300 °C with 1 °C·min^{-1}. The reaction mixture consisted of 0.3% butadiene, 30% propene, 20% hydrogen, and He for balance, and flow rate was 50 mL·min^{-1}.

3.4. Catalyst Stability. Figure 5 shows the evolution of the butadiene conversion comparing the Au/TiO_2 and Au/SiO_2-A50 catalysts at 200 °C during prolonged time-on-stream. The Au/TiO_2 is initially 2.4 times more active than the Au/SiO_2-A50. However, the Au/TiO_2 gradually loses activity from 80% to 9% conversion, hence losing 88% of its initial activity during 16 h of time-on-stream, while the Au/SiO_2-A50 is much more stable. At the first 8 h of reaction, the Au/TiO_2 catalysts exhibit close to second-order deactivation, but on longer time scales deactivation is slower than expected based on a second order dependence on the activity (Supporting Information, S.2). Stability tests at higher conversions (Figure S7), for which 150 mg of catalyst was used instead of 60 mg, confirmed that the Au/SiO_2 catalysts clearly outperform the Au/TiO_2 catalysts after several hours of reaction. The difference in catalyst stability is striking. Although it has been suggested before that the support might have an influence on the Au catalyst stability for hydrogenation reactions,[26,37] this is the first study directly comparing the stabilities of Au catalysts with similar structural properties but on different supports during extended run time.

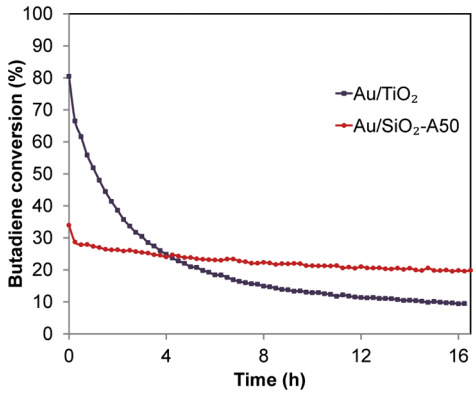

Figure 5. Evolution of the butadiene conversion comparing the Au/TiO_2 to the Au/SiO_2-A50 catalysts (both 60 mg) during the hydrogenation of butadiene at 200 °C. The reaction mixture consisted of 0.3% butadiene, 30% propene, 20% hydrogen, and He for balance, and flow rate was 50 mL·min^{-1}. The height of the catalytic beds was the same.

We will discuss first the origin of the deactivation for Au/TiO_2 before we look in detail into the stability of the SiO_2-supported Au catalysts. A common reason for activity loss in supported metal nanoparticulate catalysts is particle growth and hence loss of active metal surface area. However, in this case, EXAFS performed before and after catalysis (Figure S8 and Table S1) shows only a very slight increase in average coordination number, from 9.2 for the as-prepared Au/TiO_2 catalyst to 9.4 for the spent one, a difference which is close to or within the error margin. Also, as determined from TEM images of the spent catalysts, particle growth was not observed for both TiO_2- and SiO_2-supported catalyst. Hence, metal particle growth does not, or only to a very minor extent, contribute to the activity loss.

A second possible reason for the deactivation of the catalysts is carbonaceous deposit formation, which has been reported before as a major cause of activity loss in hydrogenation reactions.[35−39,75] By heating sample in oxygen, these carbonaceous deposits are burned off, and the weight loss can be used to quantify the extent of carbon deposition. Figure 6 shows the weight loss of the Au/SiO_2−A50 and Au/TiO_2 catalysts just before catalysis (after in situ reduction), and after catalysis. Figure 6 also shows the weight loss of the bare supports after exposure to the reaction mixture under similar conditions. The Au/SiO_2 after catalysis as well as the bare SiO_2 exposed to reaction conditions show a limited and very gradual weight loss only at temperatures above 350 °C, which is rather due to the condensation of surface hydroxyl groups than to carbon combustion. In contrast, the Au/TiO_2 after catalysis as well as the bare TiO_2 exposed to the reaction conditions show a weight loss of 2.0% at temperatures between 150 and 450 °C, which is attributed to the combustion of carbonaceous species. Interestingly the presence or absence of Au has little influence. The amount of carbonaceous species corresponds to a monolayer flat deposition of aliphatic compounds (like butadiene, assuming one molecule of butadiene occupies a surface of 20 Å^2) on the TiO_2 support (surface area of 50 m^2/g). We attribute the difference in carbon deposition to the difference in surface Lewis acidity, which is reported to lead to conversion of olefins into carbonaceous deposits.[76,77] A high number of surface groups with Lewis acidity are present on TiO_2 but not on SiO_2,[78] while also basic surface groups on the TiO_2 could contribute to the coke formation. Note that without Au, no hydrogenation products are detected in the outlet stream; hence, the carbonaceous deposits remain strongly adsorbed on the TiO_2 surface.

Although the exact nature of the active sites for hydrogenation reaction on the Au on TiO_2 catalysts is not known, it is clear that the use of a TiO_2 support induces a high initial activity, which is probably related to sites close to the Au/TiO_2 interface. It is likely that the carbon deposition rapidly deactivates these active sites especially on the small supported Au clusters and possibly via spillover also gradually other active sites on the supported Au nanoparticles. This offers an explanation for the fast activity decrease of the Au/TiO_2 catalysts at the early stage of reaction, and it explains why their activity becomes even lower than the activity of the Au/SiO_2 catalysts in the long term.

A third possible reason that might lead to deactivation especially under reducing conditions is strong-metal−support-interaction (SMSI), which means that a support under reaction conditions is partially reduced, and as a result, it has a high affinity for the metal nanoparticle and can partially or fully cover the (active) surface of metal nanoparticles. This effect is known to occur for metal particles supported on reducible

DOI: 10.1021/acscatal.7b01424
ACS Catal. 2017, 7, 5594−5603

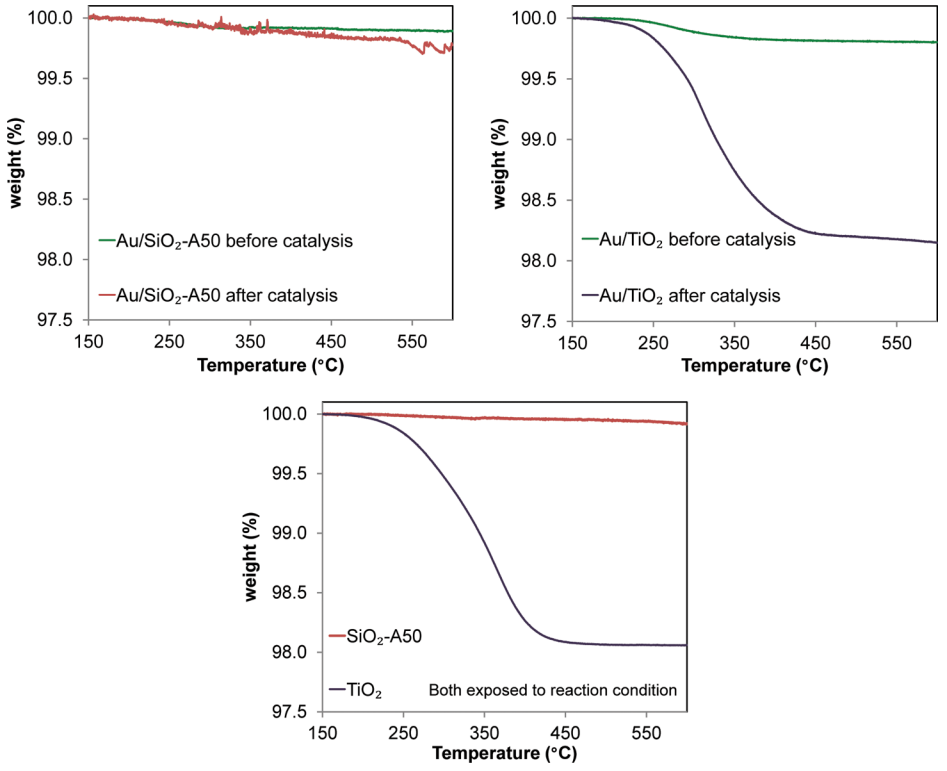

Figure 6. Weight loss upon heating with 5 °C·min^{-1} under a 10 mL·min^{-1} flow of oxygen (indicative of the amount of carbon present on the samples) for the Au/SiO_2−A50 and Au/TiO_2 catalysts before and after catalysis (top), and the results for the bare supports after exposure to the reaction mixture (bottom) under similar conditions (60 mg, for 16 h, at 200 °C). The reaction mixture consisted of 0.3% butadiene, 30% propene, 20% hydrogen, and He for balance, and the flow rate was 50 mL·min^{-1}.

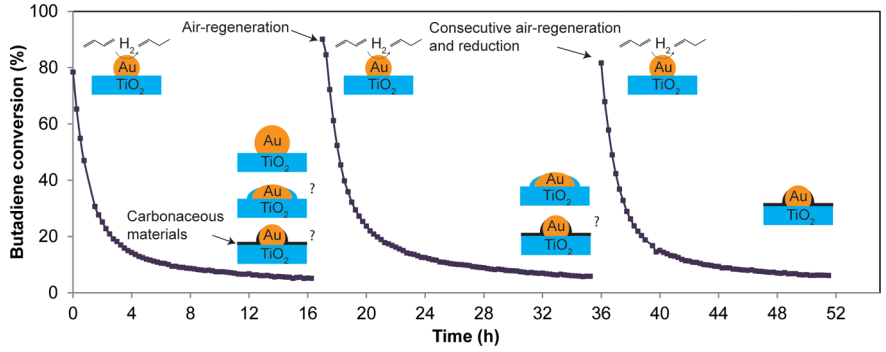

Figure 7. Evolution of the butadiene conversion during the hydrogenation of butadiene at 200 °C for, in time order, the Au/TiO_2 catalyst (60 mg), after air regeneration (50 mL·min^{-1}, at 450 °C for 1.5 h), and after consecutive air-regeneration (50 mL·min^{-1}, at 450 °C for 1.5 h) and reduction (50 mL·min^{-1}, at 450 °C for 3 h). The reaction mixture consisted of 0.3% butadiene, 30% propene, 20% hydrogen, and He for balance, and flow rate was 50 mL·min^{-1}.

supports like TiO_2 under reducing conditions at temperature higher than 477 °C.[47,79]

One of the ways to allow distinction between the different deactivation pathways is to heat the sample to high temperatures after it has lost activity due to time-on-stream. If particle growth is the main deactivation mechanism, regeneration of the activity is not expected. If deposition of carbonaceous species is the main reason for deactivation, heating to high temperatures under oxidizing atmosphere removes the carbon species (as illustrated in Figure 6) and reactivates the catalyst. If the SMSI effect is the dominant deactivation mechanism, oxidative treatment can reverse the SMSI effect,[47] but high-temperature treatment under reducing conditions is expected to enhance the SMSI effect and hence lead to a low activity.

Figure 7 shows the evolution of the butadiene conversion for the Au/TiO_2 catalyst: after 16 h on stream at 200 °C the catalyst has lost 93% of its activity. The spent catalyst is subjected to a 1.5 h air treatment at 450 °C. This treatment revives the catalytic activity, confirming that particle growth cannot be a deactivation mechanism. After renewed time-on-stream, the spent catalyst is subjected to a 1.5 h air treatment at 450 °C followed by a 3 h H_2 treatment at 450 °C. This high temperature treatment under reducing conditions leaves the catalyst fully active. It is highly unlikely that the SMSI effect does not occur at 450 °C during treatment in reductive atmosphere but would occur to a large extent at 200 °C during time-on-stream. This is in line with the literature which reports that the SMSI effect occurs only at 477 °C and above for Au/

DOI: 10.1021/acscatal.7b01424
ACS Catal. 2017, 7, 5594−5603

TiO_2.[47,79] Hence, carbon deposition is the main deactivation mechanism of the Au/TiO_2 catalyst, and it can be regenerated by burning off all carbonaceous deposits in air.

The catalyst stability is very different for the silica-based catalysts. Figure 8 shows the evolution of the butadiene conversion for the three Au/SiO_2 catalysts at 200 °C, comparing Au catalysts on the two amorphous SiO_2 supports (Aerosil 50 and 300) and on the ordered mesoporous SBA15. As discussed before, all three Au/SiO_2 catalysts showed similar intrinsic initial activities at 120 °C. Note that different initial conversions were observed in this experiment, as different amount of catalysts with different Au loadings were used. Nevertheless, a common feature that was observed for all SiO_2-supported Au catalysts that we tested is that all of them showed an excellent stability, retaining most of their initial activity during 21 h of reaction. The Au/SBA15 catalyst was even tested for 5 days and retained almost all of its initial activity (at about 90% of conversion) at this period (Figure S9). Hence, we can conclude that regardless of the support surface areas, pore structure, and conversion level, silica supports lead to exceptional long-term stability for Au catalysts for butadiene hydrogenation.

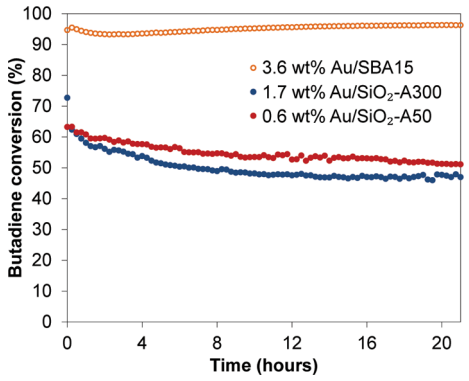

Figure 8. Evolution of the butadiene conversion for the Au/SiO_2 catalysts: Au/SBA15 (50 mg), Au/SiO_2-A300 (100 mg), Au/SiO_2-A50 (150 mg) during the hydrogenation of butadiene at 200 °C. The reaction mixture consisted of 0.3% butadiene, 30% propene, 20% hydrogen, and He for balance, and flow rate was 50 mL·min^{-1}.

CONCLUSIONS

The selectivity, activity, and stability of Au/TiO_2 and Au/SiO_2 catalysts for the selective hydrogenation of butadiene in the presence of an excess of propene were investigated. The Au/TiO_2 and Au/SiO_2 catalysts were prepared with the same method (by Au deposition on intermediate functional groups on the both supports) and showed similar structural properties (Au loading and support surface area) except for the fact that the TiO_2-supported catalysts additionally showed some smaller Au clusters. SiO_2-supported catalysts were as selective as the Au/TiO_2 catalysts but showed lower initial activities.

The TiO_2-supported catalysts showed high initial activity but rapidly lost activity during time-on-stream at 200 °C. No significant growth of the Au nanoparticles was observed, and the initial activity was readily recovered by heating in air, even if this was followed by a high temperature reductive treatment. Therefore, strong metal−support interaction was excluded as a main reason for the activity loss. Instead the deposition of carbonaceous species, facilitated by the surface properties of the TiO_2 support, was the main cause for activity loss. Probably active Au sites on the small clusters and close to the TiO_2 support are most susceptible to deactivation.

In contrast, for the SiO_2 supports, very limited coke deposition was measured under reaction conditions. Au/SiO_2 catalysts showed excellent stabilities, generally losing less than 10% of the initial activity during 5 days of run time, independent of the SiO_2 specific surface area or pore size. As a result, despite their lower initial activities, they clearly outperformed the Au/TiO_2 catalysts within several hours of run time.

ASSOCIATED CONTENT

Supporting Information

The Supporting Information is available free of charge on the ACS Publications website at DOI: 10.1021/acscatal.7b01424.

Additional details on the structural analysis (EXAFS, EDX spectroscopy, TGA, nitrogen physisorption, XRD) and catalysis results (PDF)

AUTHOR INFORMATION

Corresponding Author

*E-mail: p.e.dejongh@uu.nl.

ORCID

Petra E. de Jongh: 0000-0002-2216-2620

Notes

The authors declare no competing financial interest.

ACKNOWLEDGMENTS

We gratefully acknowledge Marjan Versluijs-Helder for TGA, Jessi van der Hoeven and Prof. Xavier Carrier for the EXAFS analysis. We acknowledge SOLEIL for provision of synchrotron radiation facilities, and we would like to thank Dr. Camille La Fontaine for assistance in using beam line ROCK which was supported by a public grant overseen by the French National Research Agency (ANR) as part of the "Investissements d'Avenir" Program (reference: ANR-10-EQPX-45). We are grateful to Utrecht University for a short stay Ph.D. fellowship and to NWO-Vici (16.130.344) for overall funding of the project. K. P. de Jong acknowledges support from the European Research Council, EU FP7 ERC Advanced Grant no. 338846. T. A. G. Silva acknowledges support from CNPq (Conselho Nacional de Desenvolvimento Científico e Tecnológico - Brazil)

REFERENCES

(1) Haruta, M.; Yamada, N.; Kobayashi, T.; Iijima, S. *J. Catal.* **1989**, *115*, 301−309.
(2) Boronat, M.; Corma, A. *Langmuir* **2010**, *26*, 16607−16614.
(3) Green, I. X.; Tang, W.; Neurock, M.; Yates, J. T., Jr. *Science* **2011**, *333*, 736−739.
(4) Zhang, Y.; Cui, X.; Shi, F.; Deng, Y. *Chem. Rev.* **2012**, *112*, 2467−2505.
(5) Ward, T.; Delannoy, L.; Hahn, R.; Kendell, S.; Pursell, C. J.; Louis, C.; Chandler, B. D. *ACS Catal.* **2013**, *3*, 2644−2653.
(6) Morfin, F.; Ait-Chaou, A.; Lomello, M.; Rousset, J.-L. *J. Catal.* **2015**, *331*, 210−216.
(7) Dong, W.; Reichenberger, S.; Chu, S.; Weide, P.; Ruland, H.; Barcikowski, S.; Wagener, P.; Muhler, M. *J. Catal.* **2015**, *330*, 497−506.
(8) Lin, J.; Abroshan, H.; Liu, C.; Zhu, M.; Li, G.; Haruta, M. *J. Catal.* **2015**, *330*, 354−361.

DOI: 10.1021/acscatal.7b01424
ACS Catal. 2017, 7, 5594−5603

(9) Priebe, J. B.; Radnik, J.; Lennox, A. J. J.; Pohl, M.-M.; Karnahl, M.; Hollmann, D.; Grabow, K.; Bentrup, U.; Junge, H.; Beller, M.; Brückner, A. *ACS Catal.* **2015**, *5*, 2137−2148.
(10) Wang, J.; Kondrat, S. A.; Wang, Y.; Brett, G. L.; Giles, C.; Bartley, J. K.; Lu, L.; Liu, Q.; Kiely, C. J.; Hutchings, G. J. *ACS Catal.* **2015**, *5*, 3575−3587.
(11) Back, S.; Yeom, M. S.; Jung, Y. *ACS Catal.* **2015**, *5*, 5089−5096.
(12) Lenz, J.; Campo, B. C.; Alvarez, M.; Volpe, M. A. *J. Catal.* **2009**, *267*, 50−56.
(13) Li, G.; Zeng, C.; Jin, R. *J. Am. Chem. Soc.* **2014**, *136*, 3673−3679.
(14) Liu, X.; Mou, C.-Y.; Lee, S.; Li, Y.; Secrest, J.; Jang, B. W. L. *J. Catal.* **2012**, *285*, 152−159.
(15) Delannoy, L.; Thrimurthulu, G.; Reddy, P. S.; Methivier, C.; Nelayah, J.; Reddy, B. M.; Ricolleau, C.; Louis, C. *Phys. Chem. Chem. Phys.* **2014**, *16*, 26514−26527.
(16) Hugon, A.; Delannoy, L.; Louis, C. *Gold Bull.* **2009**, *42*, 310−320.
(17) Wang, X.; Perret, N.; Delgado, J. J.; Blanco, G.; Chen, X.; Olmos, C. M.; Bernal, S.; Keane, M. A. *J. Phys. Chem. C* **2013**, *117*, 994−1005.
(18) Perret, N.; Wang, X.; Onfroy, T.; Calers, C.; Keane, M. A. *J. Catal.* **2014**, *309*, 333−342.
(19) Hartadi, Y.; Widmann, D.; Behm, R. J. *ChemSusChem* **2015**, *8*, 456−465.
(20) Cardenas-Lizana, F.; Gomez-Quero, S.; Idriss, H.; Keane, M. A. *J. Catal.* **2009**, *268*, 223−234.
(21) Fujitani, T.; Nakamura, I.; Akita, T.; Okumura, M.; Haruta, M. *Angew. Chem., Int. Ed.* **2009**, *48*, 9515−9518.
(22) Naito, S.; Tanimoto, M. *J. Chem. Soc., Faraday Trans. 1* **1988**, *84*, 4115.
(23) Zanella, R.; Louis, C.; Giorgio, S.; Touroude, R. *J. Catal.* **2004**, *223*, 328−339.
(24) Bus, E.; Miller, J. T.; van Bokhoven, J. A. *J. Phys. Chem. B* **2005**, *109*, 14581−14587.
(25) Boronat, M.; Illas, F.; Corma, A. *J. Phys. Chem. A* **2009**, *113*, 3750−3757.
(26) Hugon, A.; Delannoy, L.; Louis, C. *Gold Bull.* **2008**, *41*, 127−138.
(27) Bond, G. C.; Louis, C.; Thompson, D. T. In *Catalysis by Gold*; Hutchings, G. J., Ed.; Catalytic Science Series; Imperial College Press: London, 2006; Vol. *6*, pp 337−356.
(28) Denkwitz, Y.; Schumacher, B.; Kucerova, G.; Behm, R. J. *J. Catal.* **2009**, *267*, 78−88.
(29) Valden, M.; Lai, X.; Goodman, D. W. *Science* **1998**, *281*, 1647−1650.
(30) Zanella, R.; Giorgio, S.; Shin, C. H.; Henry, C. R.; Louis, C. *J. Catal.* **2004**, *222*, 357−367.
(31) Deng, W.; Flytzani-Stephanopoulos, M. *Angew. Chem., Int. Ed.* **2006**, *45*, 2285−2289.
(32) Xu, C. L.; Wang, Z.; Huangfu, X. T.; Wang, H. F. *RSC Adv.* **2014**, *4*, 27337−27345.
(33) Nijhuis, T. A.; Huizinga, B. J.; Makkee, M.; Moulijn, J. A. *Ind. Eng. Chem. Res.* **1999**, *38*, 884−891.
(34) Laveille, P.; Guillois, K.; Tuel, A.; Petit, C.; Basset, J. M.; Caps, V. *Chem. Commun.* **2016**, *52*, 3179−3182.
(35) Choudhary, T. V.; Sivadinarayana, C.; Datye, A. K.; Kumar, D.; Goodman, D. W. *Catal. Lett.* **2003**, *86*, 1−8.
(36) Yan, X. L.; Wheeler, J.; Jang, B.; Lin, W. Y.; Zhao, B. R. *Appl. Catal., A* **2014**, *487*, 36−44.
(37) Sarkany, A. *React. Kinet. Catal. Lett.* **2009**, *96*, 43−54.
(38) Azizi, Y.; Petit, C.; Pitchon, V. *J. Catal.* **2008**, *256*, 338−344.
(39) Gluhoi, A. C.; Bakker, J. W.; Nieuwenhuys, B. E. *Catal. Today* **2010**, *154*, 13−20.
(40) Nkosi, B.; Coville, N. J.; Hutchings, G. J. *J. Chem. Soc., Chem. Commun.* **1988**, 71.
(41) Cardenas-Lizana, F.; Wang, X. D.; Lamey, D.; Li, M. S.; Keane, M. A.; Kiwi-Minsker, L. *Chem. Eng. J.* **2014**, *255*, 695−704.
(42) Zanella, R.; Louis, C. *Catal. Today* **2005**, *107−108*, 768−777.
(43) Saavedra, J.; Powell, C.; Panthi, B.; Pursell, C. J.; Chandler, B. D. *J. Catal.* **2013**, *307*, 37−47.
(44) Tauster, S. J.; Fung, S. C.; Baker, R. T. K.; Horsley, J. A. *Science* **1981**, *211*, 1121−1123.
(45) Behrens, M.; Studt, F.; Kasatkin, I.; Kuhl, S.; Havecker, M.; Abild-Pedersen, F.; Zander, S.; Girgsdies, F.; Kurr, P.; Kniep, B. L.; Tovar, M.; Fischer, R. W.; Norskov, J. K.; Schlogl, R. *Science* **2012**, *336*, 893−897.
(46) Naumann d'Alnoncourt, R.; Xia, X.; Strunk, J.; Loffler, E.; Hinrichsen, O.; Muhler, M. *Phys. Chem. Chem. Phys.* **2006**, *8*, 1525−1538.
(47) Goodman, D. W. *Catal. Lett.* **2005**, *99*, 1−4.
(48) Matsubu, J. C.; Zhang, S.; DeRita, L.; Marinkovic, N. S.; Chen, J. G.; Graham, G. W.; Pan, X.; Christopher, P. *Nat. Chem.* **2016**, *9*, 120−127.
(49) *Scientific Bases for the Preparation of Heterogeneous Catalysts: Proceedings of the 10th International Symposium*, Louvain-la-Neuve, Belgium, July 11−15, 2010; Gaigneaux, E., Devillers, M., Hermans, S., Jacobs, P. A., Martens, J., Ruiz, P., Eds.; Elsevier Science: The Netherlands, 2010.
(50) van den Berg, R.; Prieto, G.; Korpershoek, G.; van der Wal, L. I.; van Bunningen, A. J.; Laegsgaard-Jorgensen, S.; de Jongh, P. E.; de Jong, K. P. *Nat. Commun.* **2016**, *7*, 13057.
(51) Sayari, A.; Han, B. H.; Yang, Y. *J. Am. Chem. Soc.* **2004**, *126*, 14348−14349.
(52) Delannoy, L.; El Hassan, N.; Musi, A.; Le To, N. N.; Krafft, J. M.; Louis, C. *J. Phys. Chem. B* **2006**, *110*, 22471−22478.
(53) Liu, X. Y.; Wang, A. Q.; Yang, X. F.; Zhang, T.; Mou, C. Y.; Su, D. S.; Li, J. *Chem. Mater.* **2009**, *21*, 410−418.
(54) Corma, A.; Garcia, H. *Chem. Soc. Rev.* **2008**, *37*, 2096−2126.
(55) Veith, G. M.; Lupini, A. R.; Rashkeev, S.; Pennycook, S. J.; Mullins, D. R.; Schwartz, V.; Bridges, C. A.; Dudney, N. J. *J. Catal.* **2009**, *262*, 92−101.
(56) Zheng, N.; Stucky, G. D. *J. Am. Chem. Soc.* **2006**, *128*, 14278−14280.
(57) Jia, C. J.; Schüth, F. *Phys. Chem. Chem. Phys.* **2011**, *13*, 2457−2487.
(58) Hugon, A.; El Kolli, N.; Louis, C. *J. Catal.* **2010**, *274*, 239−250.
(59) Delannoy, L.; El Hassan, N.; Musi, A.; Le To, N. N.; Krafft, J. M.; Louis, C. *J. Phys. Chem. B* **2006**, *110*, 22471−22478.
(60) Munnik, P.; de Jongh, P. E.; de Jong, K. P. *Chem. Rev.* **2015**, *115*, 6687−6718.
(61) Comotti, M.; Li, W. C.; Spliethoff, B.; Schuth, F. *J. Am. Chem. Soc.* **2006**, *128*, 917−924.
(62) Hartfelder, U.; Kartusch, C.; Makosch, M.; Rovezzi, M.; Sá, J.; van Bokhoven, J. A. *Catal. Sci. Technol.* **2013**, *3*, 454−461.
(63) Widmann, D.; Liu, Y.; Schüth, F.; Behm, R. J. *J. Catal.* **2010**, *276*, 292−305.
(64) Fang, J.; Li, J.; Zhang, B.; Yuan, X.; Asakura, H.; Tanaka, T.; Teramura, K.; Xie, J.; Yan, N. *Nanoscale* **2015**, *7*, 6325−6333.
(65) Mueller, R.; Kammler, H. K.; Wegner, K.; Pratsinis, S. E. *Langmuir* **2003**, *19*, 160−165.
(66) Nikitenko, S.; Beale, A. M.; van der Eerden, A. M.; Jacques, S. D.; Leynaud, O.; O'Brien, M. G.; Detollenaere, D.; Kaptein, R.; Weckhuysen, B. M.; Bras, W. *J. Synchrotron Radiat.* **2008**, *15*, 632−640.
(67) Sing, K. S. W.; Rouquer, J. In *Handbook of Heterogeneous Catalysis*; Ertl, G., Knozinger, H., Weitkamc, J., Eds.; VCH Verlagsgesellschaft mbH: Weinheim, 1997; pp 439−441.
(68) Yang, X.-F.; Wang, A.-Q.; Wang, Y.-L.; Zhang, T.; Li, J. *J. Phys. Chem. C* **2010**, *114*, 3131−3139.
(69) Okumura, M.; Akita, T.; Haruta, M. *Catal. Today* **2002**, *74*, 265−269.
(70) Zhang, X.; Shi, H.; Xu, B. Q. *Angew. Chem., Int. Ed.* **2005**, *44*, 7132−7135 reference 13 (There TOF presented by Okumura, M.; Akita, T.; Haruta, M. *Catal. Today* **2002**, *74*, 265−269 has been corrected.).

DOI: 10.1021/acscatal.7b01424
ACS Catal. 2017, 7, 5594−5603

(71) Masoud, N.; Delannoy, L.; Calers, C.; Gallet, J.-J.; Bournel, F.; de Jong, K. P.; Louis, C.; de Jongh, P. E. *ChemCatChem* **2017**, *9*, 2418−2425.
(72) Nakamura, I.; Mantoku, H.; Furukawa, T.; Fujitani, T. *J. Phys. Chem. C* **2011**, *115*, 16074−16080.
(73) Sun, K.; Kohyama, M.; Tanaka, S.; Takeda, S. *J. Phys. Chem. C* **2014**, *118*, 1611−1617.
(74) Cárdenas-Lizana, F.; Gómez-Quero, S.; Perret, N.; Keane, M. A. *Gold Bull.* **2009**, *42*, 124−132.
(75) Guisnet, M.; Magnoux, P. *Appl. Catal., A* **2001**, *212*, 83−96.
(76) *New Solid Acids and Bases—Their Catalytic Properties*; Tanabe, K.; Misono, M.; Ono, Y.; Hattor, H. Elsevier: Amsterdam, 1990; Vol. *51*.
(77) Gruia, A. In *Handbook of Petroleum Processing*; Jones, D. S. J., Pujadó, P. R., Eds.; Springer: Berlin, 2006; pp 298−300.
(78) Massa, M.; Andersson, A.; Finocchio, E.; Busca, G. *J. Catal.* **2013**, *307*, 170−184.
(79) Meyer, R.; Lemire, C.; Shaikhutdinov, S. K.; Freund, H. J. *Gold Bull.* **2004**, *37*, 72−124.

DOI: 10.1021/acscatal.7b01424
ACS Catal. 2017, 7, 5594−5603